Use of a Redox-Active Ligand to Reversibly Alter Metal Carbonyl Electrophilicity

Ivan M. Lorković, Mark S. Wrighton,* and William M. Davis

Contribution from the Department of Chemistry, Massachusetts Institute of Technology, Cambridge, Massachusetts 02139

Received October 14, 1993®

Abstract: The chelating ligand, 1,1′-bis(diphenylphosphino)cobaltocene (dppc) is used as an electrochemically tunable ligand for altering electrophilicity of the carbonyl carbon in metal carbonyl complexes. The Re carbonyl complexes $[Re(CO)_{4-n}(CH_3CN)_n dppc]^{2+/+}$, $n = 0$ (*cis*), 1 (*fac*), 2 (*cis,cis*), and [*fac*-$Re(CO)_3(NCO)dppc]^{+/0}$ were prepared and characterized in both states of charge indicated. Single crystal X-ray crystallography was performed for both states of charge of $[Re(CO)_4dppc]^{2+/+}$ with the oxidized and reduced forms crystallizing in the monoclinic space groups $C2/c$ and $P2_1/c$, respectively. The most pronounced structural difference between the two forms is the Cp(centroid)–Co distance, which is 0.09 Å longer for the reduced form. Cyclic voltammetry shows that $E_{1/2}$ for the Co(III)/Co(II) couple is 200–400 mV more positive for coordinated dppc than for the free ligand. For each CO substituted, $E_{1/2}$ becomes ~100 or 200 mV more negative for substitution by CH_3CN or NCO^-, respectively. Solution IR spectroscopy shows that ν_{CO} for the oxidized form of each species is typically ~15 cm^{-1} higher than for the reduced form, but the number and relative intensities of the carbonyl absorptions are the same. In every redox pair the oxidized species has higher reactivity with respect to nucleophilic attack at the carbonyl carbon. In CH_3CN at 25.0 °C, [*fac*-$Re(CO)_3(CH_3CN)dppc]^{+2}$ reacts with amine *N*-oxides $(CH_3)_3NO$, *N*-methylmorpholine *N*-oxide, and $(CH_3)_2(C_6H_5)NO$ ~200 times faster than [*fac*-$Re(CO)_3(CH_3CN)dppc]^+$ to form [*cis,cis*-$Re(CO)_2(CH_3CN)_2dppc]^{+2/+}$, while [*cis*-$Re(CO)_4dppc]^{+2}$ reacts with N_3^- 5400 times faster than [*cis*-$Re(CO)_4dppc]^+$ to form [*fac*-$Re(CO)_3(NCO)dppc]^{+/0}$, with $\Delta\Delta H^\ddagger$ = 3–4 kcal/mol in both cases. The ionic strength and dielectric strength dependence of the reactivity of $[Re(CO)_4dppc]^{+2/+}$ toward N_3^- were assayed to investigate electrostatic contributions to the attenuation of reactivity of $[Re(CO)_4dppc]^{+2/+}$ toward N_3^- caused by reduction of the dppc ligand.

We report the synthesis, characterization, and reactivities of rhenium carbonyl derivatives of the reversibly redox-active chelating ligand 1,1′-bis(diphenylphosphino)cobaltocene (dppc). We show that the carbonyl carbon atoms are much more electrophilic when the ligand is oxidized. Our results illustrate the concept that electroactive ligands can be used to control reactivity of the moiety to which they are bound (Scheme 1).

Reversibly redox-active centers in complex molecules have found use in a number of areas in chemistry, ranging from electrochemical sensing of small molecules[1] and ions,[2,3] where the redox potential of the ligand changes upon binding of the analyte, to the development of molecular electrocatalysts for multielectron redox processes, such as the four-electron reduction of oxygen to water,[4] for which the electroactive ligands serve to store and deliver electrons to the catalytic site. More recently, use of electroactive ligands to alter binding properties has received attention. Association constants between cationic guests and ferrocene-derived aza-crown ether hosts decrease several orders of magnitude upon oxidation of the host to ferrocenium.[2] Rate and product distribution of homogeneous Rh- and Ir-catalyzed reduction/isomerization of unsaturated functionality can be controlled by changing the state of charge of chelating metallocene-based phosphine ligands.[5] For all these functions, a high degree of communication between reactive and redox sites is important.

Scheme 1. Electrochemical Control of Metal Carbonyl Electrophilicity through the Use of a Chelating Cobaltocene-Based Phosphine Ligand

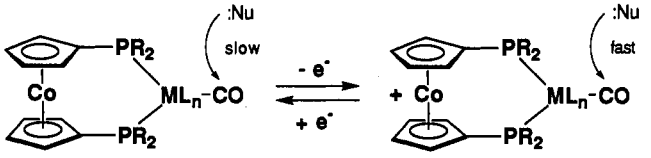

Reduced, "off" **Oxidized, "on"**

Carbon monoxide is remarkable as a ligand in its π acidity and capacity to act as an electronic "buffer" to stabilize metals in low oxidation states. The carbonyl stretching frequency (ν_{CO}) for terminally bound CO is observed anywhere from ~2200 cm^{-1} for electron-poor complexes to 1600 cm^{-1} for highly electron-rich ones, ranging over a full unit of apparent bond order. The carbon atom of CO bound to transition metals can be electrophilic,[6-12] more so for metal carbonyls with higher ν_{CO}.[7,10] These trends are

* Author to whom correspondence should be addressed.

® Abstract published in *Advance ACS Abstracts*, May 15, 1994.

(1) (a) Mirkin, C. A.; Wrighton, M. S. *J. Am. Chem. Soc.* **1990**, *112*, 8596. (b) Singewald, E. T.; Mirkin, C. A. *Abstracts of Papers*, 206th National Meeting of the American Chemical Society, Chicago, IL; American Chemical Society: Washington, DC, 1993; INOR 405.

(2) (a) Medina, J. C.; Goodnow, T. T.; Rojas, M. T.; Atwood, J. L.; Lynn, B. C.; Kaifer, A. E.; Gokel, G. W. *J. Am. Chem. Soc.* **1992**, *114*, 10583 and references therein. (b) Allgeier, A. M.; Singewald, E. T.; Mirkin, C. A. *Abstracts of Papers*, 206th National Meeting of the American Chemical Society, Chicago, IL; American Chemical Society: Washington, DC, 1993; INOR 404.

(3) (a) Beer, P. D.; Crowe, D. B.; Main, B. *J. Organomet. Chem.* **1989**, *375*, C35. (b) Beer, P. D.; Keefe, A. D. *J. Organomet. Chem.* **1989**, *375*, C40. (c) Beer, P. D.; Blackburn, C.; McAleer, J. F.; Sikanyika, H. *Inorg. Chem.* **1990**, *29*, 378. (d) Beer, P. D.; Keefe, A. D.; Sikanyika, H.; Blackburn, C.; McAleer, J. F. *J. Chem. Soc., Dalton Trans.* **1990**, 3289. (e) Beer, P. D.; Nation, J. E.; McWhinnie, S. L. W.; Harman, M. E.; Hursthouse, M. B.; Ogden, M. I.; White, A. H. *J. Chem. Soc., Dalton Trans* **1991**, 2485. (f) AlObaidi, N. J.; Salam, S. S.; Beer, P. D.; Bush, C. D.; Hamor, T. A.; McQuillan, F. S.; Jones, C. J.; McLeverty, J. A. *Inorg. Chem.* **1992**, *31*, 263. (g) Beer, P. D.; Hesek, D.; Hodacova, J.; Stokes, S. E. *J. Chem. Soc., Chem. Commun.* **1992**, 270. (h) Beer, P. D.; Drew, M. G. B.; Hazlewood, C.; Hesek, D.; Hodacova, J.; Stokes, S. E. *J. Chem. Soc., Chem. Commun.* **1993**, 229.

(4) (a) Shi, C.; Anson, F. C. *J. Am. Chem. Soc.* **1991**, *113*, 9564. (b) Shi, C.; Anson, F. C. *Inorg. Chem.* **1992**, *31*, 5078.

(5) Lorković, I. M.; Duff, R. R.; Wrighton, M. S. Manuscript in preparation.

(6) Mutterties, E. L. *Inorg. Chem.* **1965**, *4*, 1841. Darensbourg, D. J.; Drew, D. *J. Am. Chem. Soc.* **1976**, *98*, 275.

0002-7863/94/1516-6220$04.50/0

Scheme 2. Increased d to π^* "π-Backbonding" Decreases Carbon Electrophilicity and ν_{CO}

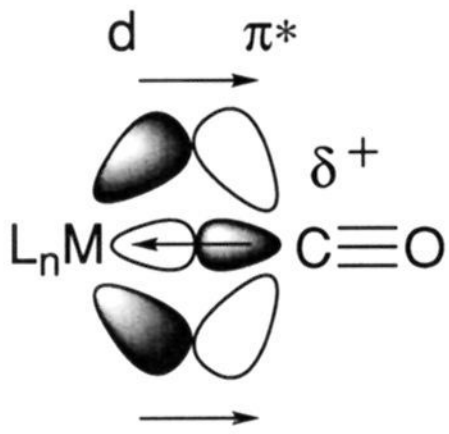

understood in terms of the degree of π back-donation from metal-d to CO-π^* orbitals (Scheme 2).

There is evidence that carbonyl carbon electrophilicity and ν_{CO} can be electrochemically tuned. Weaver and co-workers have observed that, in electrolyte solution, ν_{CO} for terminally bound CO on Pt electrodes increases in a linear fashion with the potential applied to the electrode.[13a] Spectroelectrochemistry performed on high-nuclearity $Pt_n(CO)_m$ clusters mirrors this behavior in a series of up to 10 discrete states of charge.[13b] The electrophilicity of the carbonyl carbon in both of these cases changes accordingly with potential as shown by the fact that in aqueous media at high potentials and more positive states of charge electrode/cluster bound CO undergoes nucleophilic attack by water followed by electrooxidation to CO_2.[14]

Previous workers in this group and others have shown that ν_{CO} values of transition metal carbonyl complexes with ligands containing electroactive ferrocene moieties can be reversibly increased by up to 25 cm^{-1} in a one-electron oxidation of ferrocene.[15] As has been shown for CO bound to a Pt electrode, a potential dependent continuous range of CO stretching frequencies has been demonstrated for metal carbonyl derivatives covalently bound to electrochemically polymerized thiophene derivatives incorporating a metal binding pyridine group, with ν_{CO} increasing with potential as charge is drawn out of the polymer.[16]

A quantitative correlation between ν_{CO} and reactivity with respect to nucleophilic attack at the CO carbon has been obtained for a series of tungsten carbonyl derivatives containing phosphines of varying basicity.[10b] This type of correlation could also be established or tested by use of an electroactive ligand which provides an electrochemical means to a change in ligand donating ability and ν_{CO}. Cobaltocene-derived phosphines[17] are ideal electroactive ligands for such a study because cobaltocene derivatives can be durable in two states of charge in nucleophilic media. Thus, ligand decomposition should not interfere with measurements of CO reactivity. Furthermore, cobaltocene derivatives undergo minimal steric change upon oxidation, so that any change in reactivity observed will not likely be due to some change in the geometry of the complex leading to a more or less sterically hindered transition state, but rather will only reflect changed electronic factors or electrostatic effects.

Amine *N*-Oxides and N_3^- are good nucleophiles for performing reactivity studies with metal carbonyls because they react selectively and irreversibly with metal bound CO following a second-order rate law consistent with a bimolecular mechanism, as shown in eqs 1 and 2.[9,11,12] The rate determining step in both

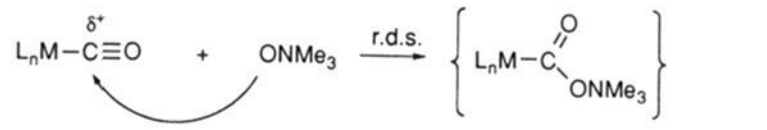

$$\xrightarrow[-CO_2,\ NMe_3]{+\ L'} L_nM-L' \qquad (1)$$

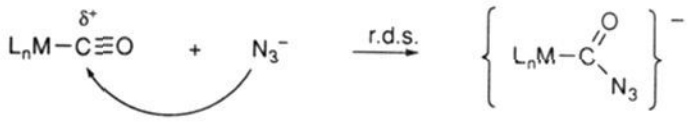

$$\xrightarrow[-N_2]{} [L_nM-NCO]^- \qquad (2)$$

cases is thought to be nucleophilic attack at the carbonyl carbon atom. R_3NO yields an open coordination site, R_3N, and CO_2 while azide yields the metal isocyanate and N_2. We establish in this paper that dppc can be used as an electrochemically tunable ligand to control electrophilicity (toward N_3^- and R_3NO) of the cationic Re(I) carbonyl moiety to which it is bound.

Experimental Section

Unless otherwise stated, all air sensitive procedures were carried out under an Ar atmosphere using standard Schlenk techniques or in a Vacuum Atmospheres drybox. CH_2Cl_2 and C_2H_5CN were distilled from P_2O_5. THF and Et_2O were heated under reflux over Na/benzophenone until purple and then distilled. Diglyme and CH_3CN were Aldrich Sureseal. $[n\text{-}Bu_4N]PF_6$ (Aldrich) was recrystallized twice from MeOH and dried *in vacuo* overnight at 120 °C. $[n\text{-}Bu_4N]N_3$ (American Tokyo Kasei) was dried in vacuo overnight at 80 °C. $(CH_3)_3NO$ was purchased (Aldrich) as the dihydrate, dried by Dean Stark techniques, and sublimed. *N*-Methylmorpholine *N*-oxide (Aldrich) was sublimed. *N,N*-Dimethylaniline *N*-oxide was prepared by literature techniques[18] and purified by sublimation followed by recrystallization from dry CH_2Cl_2/Et_2O.

NMR spectra were recorded on either a Bruker 250-MHz or Varian 300-MHz spectrometer using deuterated solvents at 25 ± 5 °C. All chemical shifts are given in ppm relative to TMS. Solution IR spectra were obtained in sealed CaF_2 or NaCl cells (0.2 or 0.1 mm) on a Nicolet 60SX FTIR spectrometer with 2-cm^{-1} resolution. Elemental analyses were performed by Galbraith Laboratories, Knoxville, TN, and Schwartzkopf Laboratories, Woodside, NY. X-ray crystallography was performed on an Enraf-Nonius CAD-4 diffractometer at either ambient conditions ($\mathbf{2}_{ox}$) or 201 K under N_2 ($\mathbf{2}_{red}$) and solved by direct methods. Further

(7) Angelici, R. J. *Acc. Chem. Res.* **1972**, *5*, 335. Angelici, R. J.; Brink, R. W. *Inorg. Chem.* **1973**, *12*, 1067. Angelici, R. J.; Blacik, L. J. *Inorg. Chem.* **1972**, *11*, 1754.

(8) Kruck, T.; Noack, M. *Chem. Ber.* **1964**, *97*, 1693.

(9) (a) Beck, W.; Smedal, H. S. *Angew. Chem.* **1966**, *78*, 267. (b) Beck W.; Smedal, H. S. *Angew. Chem., Int. Ed. Engl.* **1966**, 5253. (c) Werner, H.; Beck, W.; Engelmann, H. *Inorg. Chim. Acta* **1969**, *3*, 331. (d) Graziani, M.; Bussetto, L.; Palazzi, A. *J. Organomet. Chem.* **1971**, *26*, 261.

(10) (a) Darensbourg, D. J.; Darensbourg, M. Y. *Inorg. Chem.* **1970**, *9*, 1691. (b) Darensbourg, M. Y.; Conder, H. L.; Darensbourg, D. J.; Hasday, C. *J. Am. Chem. Soc.* **1973**, *95*, 5919. (c) Dobson, G. R.; Paxson, J. R. *J. Am. Chem. Soc.* **1973**, *95*, 5925.

(11) (a) Hieber, W.; Lipp, A. *Chem. Ber.* **1959**, *92*, 2085. (b) Alper, H.; Edward, J. T. *Can. J. Chem.* **1970**, *8*, 1543.

(12) (a) Shi, Y.-L.; Gao, Y.-C.; Shi, Q.-Z.; Kershner, D. L.; Basolo, F. J. *Organometallics* **1987**, *6*, 1528. (b) Shen, J.-K.; Gao, Y.-C.; Shi, Q.-Z.; Basolo, F. J. *J. Organomet. Chem.* **1991**, *401*, 295. (c) Shi, Y.-L.; Gao, Y.-C.; Shi, Q.-Z.; Rheingold, A. R.; Basolo, F. J. *Inorg. Chem.* **1991**, *30*, 1868.

(13) (a) Lewis, G. J.; Roth, J. D.; Montag, R. A.; Safford, L. K.; Gao, X.; Chang, S. C.; Dahl, L. F.; Weaver, M. J. *J. Am. Chem. Soc.* **1990**, *112*, 2831. (b) Roth, J. D.; Lewis, G. D.; Safford, L. K.; Jiang, X.; Dahl, L. F.; Weaver, M. J. *J. Am. Chem. Soc.* **1992**, *114*, 6159.

(14) For example, Leung, L.-W. H.; Wieckowski, A.; Weaver, M. J. *J. Phys. Chem.* **1988**, *92*, 6985. Chang, S.-C.; Leung, L.-W. H.; Weaver, M. J. *J. Phys. Chem.* **1989**, *93*, 5341.

(15) (a) Elschenbroich, C.; Stohler, F. *Angew. Chem., Int. Ed. Engl.* **1975**, *14*, 174. (b) Kotz, J. C.; Nivert, C. L.; Lieber, J. M.; Reed, R. C. *J. Organomet. Chem.* **1975**, *91*, 87. (c) Colbron, S. B.; Robinson, B. H.; Simpson, J. *Organometallics* **1983**, *2*, 943. (d) Miller, T. M.; Ahmed, K. J.; Wrighton, M. S. *Inorg. Chem.* **1989**, *28*, 2347.

(16) Wolf, M. O.; Wrighton, M. S. Submitted to *Chem. Mat.*, 1994.

(17) (a) Rudie, A. W.; Lichtenberg, D. W.; Katcher, M. L.; Davison, A. *Inorg. Chem.* **1978**, *17*, 2859. (b) Dubois, D. L.; Eigenbrot, C. W., Jr.; Miedaner, A.; Smart, J. C. *Organometallics* **1986**, *5*, 1405.

(18) Craig, J. C.; Purushothaman, K. K. *J. Org. Chem.* **1970**, *35*, 1721.

experimental details are presented as supplementary material. Electronic absorption spectra were recorded on a Hewlett-Packard 8452a diode array spectrophotometer. Electrochemical measurements were performed using a Pine Instruments model RDE-4 potentiostat with a Kipp and Zonen XY recorder, in a 0.1 M CH_3CN solution of $[n\text{-}Bu_4N]PF_6$ with Ag wire, Pt flag, and Pt gauze as quasireference, working, and counter electrodes, respectively. Ferrocene was added as an internal reference. Electrodes were cleaned by dipping in a freshly prepared solution of "piranha etch" (one part 30% aqueous H_2O_2 and three parts concentrated H_2SO_4; ***Caution***, strong oxidizer! Explosion hazard!), rinsing consecutively in H_2O and CH_3CN, and blowing dry.

Reaction rates of $\mathbf{2}_{red}$ with N_3^- and **3** with amine *N*-oxides were measured using an Applied Photophysics RX1000 rapid kinetics accessory stopped flow apparatus interfaced to the spectrophotometer and a Lauda RC-6 constant-temperature bath. The temperature was allowed to equilibrate for at least 15 min after the constant-temperature bath had reached the desired temperature. For all reduced species, the drive syringes of the stopped flow apparatus were loaded in the drybox after having degassed the apparatus under active vacuum in the drybox antechamber for at least 12 h. The constant-temperature bath was purged with Ar for at least 30 min prior to connection of the bath hoses to the stopped flow apparatus and for the duration of the experiment. Rates were measured at different temperatures in a random progression. The plots of $|A_t - A_\infty|$ versus time were fit for at least three half-lives ($R > 0.995$) using commercial spreadsheet exponential least-squares fitting software.

The reaction of $\mathbf{2}_{ox}$ (typically 10–20 μM) with N_3^- (210–1000 μM) was followed using an Applied Photophysics DX-17 stopped flow apparatus which fit the absorbance rise curve for at least three half-lives ($R > 0.995$, except for the fastest rates measured (low ionic strength data at $T > 33$ °C or low dielectric strength data; $V(C_2H_5CN) \geq 20\%$), for which $R > 0.95$) at 254 nm upon acquisition. The reaction between $\mathbf{2}_{red}$ (50–100 μM) and N_3^- (1000–3500 μM) was followed using the difference of average absorbances between 300 and 460 nm (rise) and between 500 and 650 nm (decay). The reaction between $\mathbf{3}_{ox}$ (10–20 μM) and the aliphatic amine *N*-oxides (500–2500 μM) was followed using the difference of the average absorbances between 234 and 246 nm (decay) and between 250 and 300 nm (rise), and for *N,N*-dimethylaniline *N*-oxide, by monitoring only the rise between 250 and 300 nm. The same reaction involving $\mathbf{3}_{red}$ (100–150 μM, $[R_3NO]$ = 5–25 mM) was followed, employing a 320-nm cutoff filter to protect the photosensitive solution, by monitoring the difference in the average absorbances between 390 and 460 nm (rise) and between 480 and 600 nm (decay). For all reactions, the concentration of N_3^- or amine *N*-oxide used was at least 20 times the concentration of **2** or **3**.

Syntheses. ***fac*-Re(CO)$_3$(dppc)Br]PF$_6$ (1).** Diglyme (15 mL) was added to a flask charged with $Re(CO)_5Br$ (406 mg, 1.00 mmol) and 1,1′-bis(diphenylphosphino)cobaltocenium hexafluorophosphate ([dppc]-PF_6)[17] (702 mg, 1.00 mmol) and containing a magnetic stir bar. The contents were then heated at 105 °C and stirred until CO evolution stopped (~30 min). After cooling, the precipitated light yellow solid (940 mg, 90%) was collected by filtration in air and rinsed with Et_2O. ^{1}H-NMR in acetone-d_6: δ 5.87 br (2H), 6.02 br (2H), 6.20 br (2H), 6.80 br (2H), 7.5–7.8 m (20H).

[*cis*-Re(CO)$_4$(dppc)][PF$_6$]$_2$ ($\mathbf{2}_{ox}$). Under a CO atmosphere, CH_2Cl_2 (20 mL) was added with stirring to a flask charged with **1** (500 mg, 0.47 mmol) and $AgPF_6$ (500 mg, 2 mmol), forming a lemon yellow suspension. Stirring was continued under CO (1.2 atm) for 4 h. Solvent was removed *in vacuo*, CH_3CN added, and the suspension filtered to remove AgBr. The CH_3CN was removed *in vacuo* and CH_2Cl_2 added to the yellow residue, inducing crystallization. The supernatant was decanted and the solid rinsed twice more with CH_2Cl_2, the supernatant and rinsings saved. Analytically pure lemon yellow needles of $\mathbf{2}_{ox}$ were obtained by dissolution in a minimum of CH_3CN, filtration through a pipette containing Celite, addition of 2 volumes of CH_2Cl_2, and slow diffusion of 10 volumes of Et_2O added carefully over the top. The solvent was removed from the previously saved supernatant and the residue recrystallized as described above (overall yield ca. 50%). ^{1}H-NMR (in acetone-d_6): δ 6.33 br (4H), 6.40 br (4H), 7.75 m (20H). Elemental analysis: calcd C 39.84, H 2.46; found C 40.13, H 2.59.

[*cis*-Re(CO)$_4$(dppc)]PF$_6$ ($\mathbf{2}_{red}$). In the drybox, a solution of cobaltocene (10 mg, 0.053 mmol) in CH_2Cl_2 (2 mL) was added dropwise to a stirred suspension of $\mathbf{2}_{ox}$ (63 mg, 0.055 mmol) in CH_2Cl_2 (2 mL). The resulting dark violet solution containing suspended insoluble cobaltocenium hexafluorophosphate was loaded onto a column of silica gel/CH_2Cl_2. The product was eluted with a 5:95 THF:CH_2Cl_2 mixture. The violet fraction was collected and the solvent removed. Recrystallization from CH_2Cl_2/hexanes yielded black crystals containing 0.5–1 equiv of CH_2Cl_2 (yield > 90%). Elemental analysis for a sample of $\mathbf{2}_{red}$ found by ^{1}H-NMR to contain 0.75 equiv CH_2Cl_2: calcd C 43.72, H 2.79, Cl 5.00; found C 43.89, H 2.73, Cl 5.29.

[*fac*-Re(CO)$_3$(CH$_3$CN)(dppc)][PF$_6$]$_2$ ($\mathbf{3}_{ox}$). **Method A.** To a flask charged with $\mathbf{2}_{ox}$ (500 mg, 0.47 mM) and $AgPF_6$ (500 mg, 1.98 mmol) was added CH_2Cl_2 (10 mL), followed by CH_3CN (100 μL). The light yellow suspension was allowed to stir for 5 h and then filtered through a bed of Celite. After the solvent was removed *in vacuo*, the residue was chromatographed on a column of silica gel, eluting with a mixture of CH_2Cl_2, CH_3CN, and toluene (10:2:1) (yield 80%). Attempted recrystallization of $\mathbf{3}_{ox}$ from various solvent systems always resulted in the precipitation of an amorphous solid which gave analytically pure $\mathbf{3}_{ox}$ after extensive evacuation. ^{1}H-NMR in acetone-d_6: δ 2.33 s (3H), 6.2–6.4 m (8H), 7.6–7.8 m (20H). Elemental Analysis: calcd C 40.43, H 2.69; found C 40.21, H 2.78.

Method B. A solution of $(CH_3)_3NO$ (10 mg, 0.13 mmol) in CH_3CN (5 mL) was added dropwise to a vigorously stirred solution of $\mathbf{2}_{ox}$ (153 mg, 0.13 mmol) in CH_3CN (15 mL) cooled in an ice bath. After the solvent was removed *in vacuo*, the residue was chromatographed as above.

[*fac*-Re(CO)$_3$(CH$_3$CN)(dppc)]PF$_6$ ($\mathbf{3}_{red}$). Method A. In the drybox, using only a red darkroom light for illumination, a solution of $(CH_3)_3NO$ (5.0 mg, 0.067 mmol) in CH_3CN (2 mL) was added dropwise to a stirred solution of $\mathbf{2}_{red}$ (67 mg, 0.067 mmol). A color change to brick red was noted when the addition was complete. The solvent was removed *in vacuo*, the residue was redissolved in a minimum of CH_2Cl_2 and transferred to a vial, and 3 volumes of Et_2O were layered on top. The vial was kept in the dark until crystallization was complete, giving brick red, analytically pure needles of $\mathbf{3}_{red}$ (60 mg, 90%), which incorporated approximately 1 equiv of CH_2Cl_2 by ^{1}H-NMR. Elemental analysis: calcd C 43.73, H 3.03, Cl, 6.45; found C 44.03, H 2.85, Cl 6.75. High-resolution fast atom bombardment mass spectrometry: calcd molecular ions (two major isotopes of Re) 867.064 06, 869.066 85; found 867.0646, 869.0673.

Method B. In the drybox, illuminated by only red light, a solution of cobaltocene (10 mg, 0.053 mmol) in CH_2Cl_2 (2 mL) was added dropwise to a stirred suspension of $\mathbf{3}_{ox}$ (60 mg, 0.052 mmol) in CH_2Cl_2 (2 mL). The resulting solution was loaded onto a column of silica gel, eluting first with CH_2Cl_2 to remove any excess cobaltocene and thereafter with CH_2Cl_2:THF (10:1) to elute the dark red band. The recovered solution was purified as in method A.

[*fac*-Re(CO)$_3$(NCO)(dppc)]PF$_6$ ($\mathbf{4}_{ox}$). A solution of $[(n\text{-}Bu)_4N]N_3$ (20 mg, 0.070 mmol) in CH_3CN (1 mL) was added dropwise to a solution of $\mathbf{2}_{ox}$ (83 mg, 0.072 mmol) in CH_3CN (1 mL) accompanied by gas evolution and a color change to deeper yellow. After the solvent was removed *in vacuo*, the product was separated from the $[(n\text{-}Bu)_4N]PF_6$ impurity by loading a CH_2Cl_2 solution of the yellow residue onto a column of silica gel and eluting extensively with CH_2Cl_2, first pure and then with increasing percentages of added THF. Recrystallization from CH_2Cl_2/Et_2O gave analytically pure $\mathbf{4}_{ox}$. ^{1}H-NMR in acetone-d_6: δ 5.95 br (2H), 6.11 br (2H), 6.25 br (2H), 6.42 br (2H), 7.5–7.9 m (20H). Elemental analysis: calcd C 44.98, H 2.78; found C 44.92, H 2.72.

***fac*-Re(CO)$_3$(NCO)(dppc) ($\mathbf{4}_{red}$).** In the drybox, solutions of $[(n\text{-}Bu)_4N]N_3$ (20 mg, 0.070 mmol) and cobaltocene (14 mg, 0.074 mmol), each in CH_2Cl_2 (1 mL), were sequentially added dropwise to a stirred solution of $\mathbf{2}_{ox}$ (80 mg, 0.070 mmol) in CH_3CN producing an amber solution. The solvent was removed *in vacuo*, and the residue was dissolved in CH_2Cl_2 and loaded onto a column of silica gel/CH_2Cl_2. Any excess cobaltocene was eluted with CH_2Cl_2. A mixture of 95:5 CH_2Cl_2:THF was used to elute the deep amber product. The solids isolated by evaporation of the amber fraction were found to contain $[(n\text{-}Bu)_4N]PF_6$ impurity. The impure solid was dissolved in a mixture of CH_2Cl_2 and CH_3CN and the solvent volume reduced *in vacuo* until a red-brown solid precipitated. Decanting the solvent, rinsing the solid further with CH_3CN, and recrystallization from CH_2Cl_2/hexanes gave analytically pure $\mathbf{4}_{red}$ (50 mg, 82%). Elemental analysis: calcd C 52.48, H 3.25; found C 52.30, H 3.29. High-resolution EIMS: calcd molecular ions for the two major isotopes of Re 868.035 50, 870.038 29, found 868.0362, 870.0389.

[*cis*,*cis*-Re(CO)$_2$(CH$_3$CN)$_2$(dppc)][PF$_6$]$_2$ ($\mathbf{5}_{ox}$). A solution of $(CH_3)_3NO$ (13.1 mg, 0.175 mmol) in CH_3CN (1 mL) was added dropwise, with a deepening of the yellow color, to a stirred solution of $\mathbf{2}_{ox}$ (100 mg, 0.087 mmol) in CH_3CN (5 mL). The solvent was removed, and the residue was redissolved in CH_2Cl_2 and loaded onto a column of silica gel/CH_2Cl_2, eluting with CH_2Cl_2:CH_3CN:toluene (10:2:1). Attempts at crystallization were unsuccessful, yielding only an amorphous orange-yellow solid. Analytically pure $\mathbf{5}_{ox}$ was recovered by extensive evacuation of the

Scheme 3. Synthesis of 1, 2, and 3

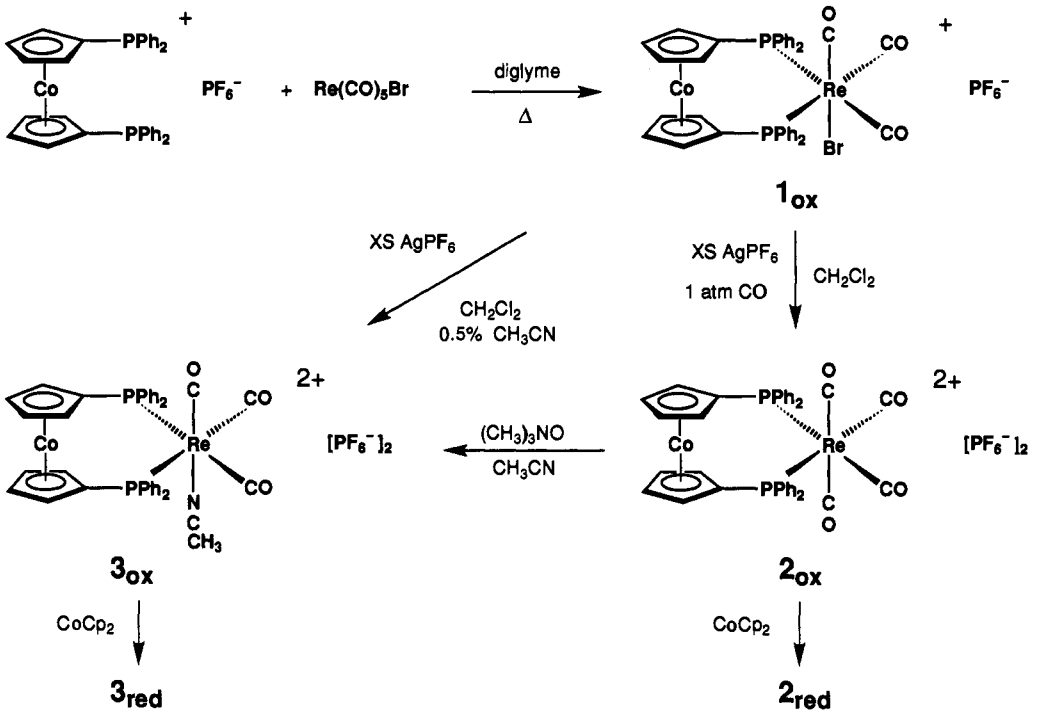

chromatographed material. The assignment of the racemic *cis–cis* structure follows from its ^{1}H-NMR spectrum, which demonstrates that all eight cyclopentadienyl protons and two sets of bound CH_3CN protons are inequivalent. ^{1}H-NMR in acetone-d_6: δ 2.23 s (3H), 2.47 s (3H), 6.09–6.19 m (6H), 6.29 br (1H), 6.36 br (1H), 7.5–7.8 m (20H). Elemental analysis: calcd C 41.00, H 2.92, found C 40.57, H 2.89.

[*cis,cis*-Re(CO)$_2$(CH$_3$CN)$_2$(dppc)]PF$_6$ (5_{red}). Synthetic procedures analogous to methods A and B for making 3_{red} were performed, including the use of only a red darkroom lamp for illumination. The product was isolated as a brownish yellow amorphous solid which, when chemically oxidized with 2_{ox}, displayed spectral properties identical to 5_{ox}. High-resolution FABMS: calcd molecular ions (two major isotopes of Re) 880.0957, 882.09849; found 880.0950, 882.0989.

Results and Discussion

The synthesis of [*fac*-Re(CO)$_3$(Br)dppc]$^{+/0}$ (**1**), [*cis*-Re(CO)$_4$dppc]$^{2+/+}$ (**2**), and [*fac*-Re(CO)$_3$(CH$_3$CN)dppc]$^{2+/+}$ (**3**) is represented in Scheme 3. To insure a good yield of 2_{ox} or 3_{ox} from the debromination of **1** in the presence of CO, it is essential that a large excess of $AgPF_6$ be used and that the mixture be stirred under CO for at least 4 h. In a test of the durability of dppc$^+$ to the nucleophiles in this study, we found that CD_3CN solutions of [dppc]PF_6 (0.1 M) with [*n*-Bu$_4$N]N_3 (0.13 M) or $(CH_3)_3NO$ (0.3 M) showed no reaction after 30 min at 25 °C. **2** reacts with either N_3^- or $(CH_3)_3NO$ (the latter at a rate we found too fast to measure ($k_2 > 5 \times 10^6$ M^{-1} s^{-1})) in CH_3CN to form [*fac*-Re(CO)$_3$(dppc)(NCO)]$^{+/0}$ (**4**) or **3**, respectively. **3** reacts further with $(CH_3)_3NO$ with replacement of a second CO to form racemic [*cis,cis*-Re(CO)$_2$(CH$_3$CN)$_2$(dppc)]$^{2+/+}$ (**5**). The important feature of the reactions of **2** and **3** with N_3^- or $(CH_3)_3NO$ is that the same reaction occurs at the Re center regardless of the state of charge of the dppc ligand, allowing the comparison of the relative reactivities of the two states of charge of complexes **2** and **3**.

Crystal Data. Despite the large number of publications describing redox activity of metallocene-containing molecules, relatively few include crystal structures of the species in both states of charge.[19] We undertook the crystallography of 2_{ox} and 2_{red} to conclusively show that reduction of the ligand causes no major changes in the geometry of ligands about Re and that the steric hindrance experienced by attacking nucleophiles is comparable for both states of charge of **2**.

Figure 1 shows the ORTEP diagrams of 2_{ox} and 2_{red}, with notable structural features shown in Table 1. Atom positional parameters and more extensive lists of bond lengths and angles are available as supplementary material. In both structures the Re and Co atoms are separated by 4.4 Å. For 2_{red}, the average Cp-centroid to Co distance is 1.715 Å, in agreement with the values calculated from the reported structures of dppc and [W(CO)$_5$]$_2$dppc (1.715 and 1.716 Å),[17b] and 0.09 Å longer than for 2_{ox}. This difference is longer than what has been observed for ferrocene/ferrocenium, for which the Fe to Cp–centroid distance typically increases by 0.06 Å upon oxidation to the 17-electron species,[19-22] and cobaltocene/cobaltocenium, for which the Co–Cp distance typically increases by 0.07 Å upon reduction to the 19-electron cobaltocene.[23,24] To summarize the structural comparison between 2_{ox} and 2_{red}, it is clear that the structures are nearly the same, but by no means superimposable. Besides the Co–Cp distance, other differences in solid-state structure between 2_{ox} and 2_{red} are likely removed by interconversion between ligand conformations, as born out by the high-symmetry ^{1}H-NMR spectra (*vide supra*) and the striking similarity in the solution IR spectra in the CO region (*vide infra*) of 2_{ox} and 2_{red}.

Electrochemistry. While most of this paper concerns changes in a metal carbonyl center induced by gain or loss of an electron at Co, shifts in the redox potential of the ligand induced by changes in the coordination sphere of the Re center are also of great interest and demonstrate in a complementary fashion electronic and/or electrostatic communication between reactive and redox sites. The free dppc ligand has a reduction potential about 200 mV more positive than that of cobaltocene, while the potential of the ligand when bound to the Re complexes studied here results in a further anodic shift of 230 mV for **5** up to 450 mV for **2**. The

(19) Gallucci, J. C.; Opromolla, G.; Paquette, L. A.; Pardi, L.; Schirch, P. F. T.; Sivik, M. R.; Zanello, P. *Inorg. Chem.* **1993**, *32*, 2292 and references therein.

(20) Cullen, W. R.; Kim, T. J.; Einstein, F. W. B.; Jones, T. *Organometallics* **1985**, *4*, 346.

(21) Seiler, P.; Dunitz, J. D. *Acta Crystallogr.* **1979**, *B35*, 1068.

(22) (a) Webb, R. J.; Lowery, M. D.; Shiomi, Y.; Sorai, M.; Wittebort, R. J.; Hendrickson, D. N. *Inorg. Chem.* **1992**, *31*, 5211. (b) Mammano, N. J.; Zalkin, A.; Landers, A.; Rheingold, A. L. *Inorg. Chem.* **1977**, *16*, 297.

(23) Bünder, W.; Weiss, E. *J. Organomet. Chem.* **1975**, *92*, 65.

(24) Churchill, M. R.; DeBoer, B. G. *J. Am. Chem. Soc.* **1974**, *96*, 6310.

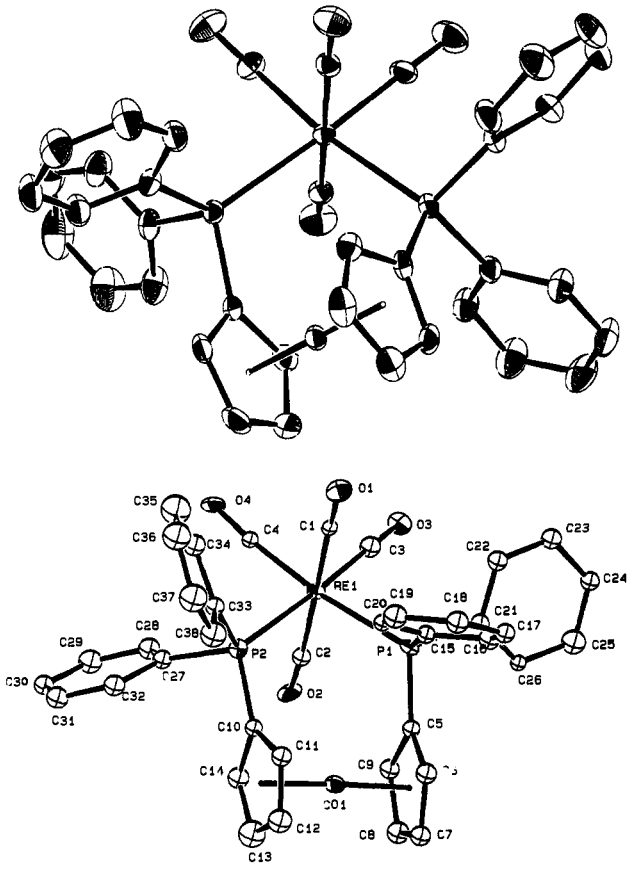

Figure 1. ORTEP diagrams of 2_{ox} (top) and 2_{red} (bottom) with ellipsoids drawn at the 35% probability level. In the bottom drawing ellipsoids without octant shading represent carbon atoms, all of which were refined only isotropically.

Table 1. Key Bond Distances (Å) and Angles (deg) in the Crystal Structures of 2_{ox} and 2_{red}

	2_{ox}	2_{red}
Re–Co	4.402(1)	4.394(3)
Co–Cp(centroid)	1.628(3)	1.72(1), 1.71(1)
Re–P	2.502(1)	2.501(6), 2.496(6)
Re–Cl, Re–C2	1.996(6)	1.96(2), 2.03(2)
Re–C3, Re–C4	1.953(6)	2.00(3), 1.91(2)
C1–Re–C2	172.6(3)	179.1(9)
C3–Re–C4	87.5(3)	85.6(9)
P–Re–P	99.70(6)	95.7(2)
Cp stagger	44	21.8

$E_{1/2}$ values for the Co(III)/Co(II) couple are included in Table 2. Replacement of one CO ligand on Re with NCO^- or Br^- results in a negative shift in the redox potential of 180 and 200 mV, respectively, while substitution by CH_3CN leads to a negative shift of 100 mV for each CO substituted. Thus, the ligand reduction potential is sensitive to the coordination environment of the Re.

Although under the right conditions cobaltocene can be stable in up to four states of charge, dication (d^5) to anion (d^8),[25] in CH_3CN at 23 °C, only the middle two are durable. Under these conditions, we observe a second wave associated with the Co(II)/Co(I) couple, reversible at scan rates down to 10 mV/s for complexes **3**, **4**, and **5** but quasireversible for the free ligand and irreversible for **1** and **2** at potentials ~900 mV more negative than the Co(III)/Co(II) wave, consistent with established trends.[25] The electrochemical reversibility of the Co(II)/Co(I) couple for complexes in which dppc binds as a chelate has been explained in terms of a template effect which holds the otherwise dissociation prone cobaltocene anion intact.[9b] Attempted preparation of the doubly reduced form of **3** by chemical reduction using decamethylcobaltocene in THF led to decomposition. For **2**, the Co(I)/Co(II) wave is followed by an irreversible two-electron reduction assignable to the Re(I)/Re(–I) couple.

(25) Bard, A. J.; Garcia, E.; Kukharenko, S.; Strelets, V. V. *Inorg. Chem.* **1993**, *32*, 3528.

Table 2. Spectroscopic and Electrochemical Data in CH_3CN at 23 ± 3 °C

		IR	UV/vis
compd	$(E_{1/2}, V)^a$	ν_{CO}, cm^{-1} (ϵ, M^{-1} cm^{-1})	λ, nm (ϵ, M^{-1} cm^{-1})^b
$CoCp_2^+$	(–1.34)		404 (208, p)
			362 (110, v)
			300 (1 060, p)
			292 (1 020, v)
			262 (33 000, p)
			228 (777, v)
$CoCp_2$			480 (110, s)
			400 (430, s)
			326 (6 700, p)
			286 (1 800, v)
			260 (6 100, p)
			244 (5 800, v)
			218 (17 000, p)
$dppc^+$	(–1.14, –2.02 (q))		378 (4 030, p)
			332 (2 490, v)
			268 (23 200, s)
			248 (27 000, p)
			232 (23 300, v)
dppc			450 (1 200, s)
			344 (4 300, p)
			332 (3 900, v)
			250 (24 000, p)
			238 (22 000, v)
1	(–0.91)		
2_{ox}	(–0.71, –1.58 (i), –1.86 (i, 2e⁻))	2 121 (1 940)	412 (408, s)
		2 049 (1 750)	274 (17 000, p)
		2 022 (4 140)	254 (13 000, v)
			222 (67 000, s)
2_{red}		2 110 (1 960)	566 (1 200, p)
		2 032 (1 870)	468 (820, v)
		2 006 (4 010)	420 (980, s)
			326 (4 800, p)
			312 (4 600, v)
			274 (10 800, s)
3_{ox}	(–0.80, –1.70)	2 062 (3 040)	274 (21 500, p)
		1 991 (1 800)	260 (19 200, v)
		1 953 (1 500)	236 (40 500, s)
3_{red}		2 048 (3 540)	478 (1 140, p)
		1 970 (2 040)	400 (760, v)
		1 940 (1 700)	316 (4 130, s)
4_{ox}[c]	(–0.89, –1.82)	2 237 (1 500, ν_{NCO})	420 (510, s)
		2 046 (3 900)	274 (18 800, p)
		1 973 (2 250)	252 (19 800, s)
		1 925 (2 300)	234 (36 900, s)
4_{red}[c]		2 245 (1 900, ν_{NCO})	460 (1 300, p)
		2 032 (3 800)	400 (1 000, v)
		1 950 (2 100)	328 (5 600, s)
		1 906 (2 000)	302 (7 350, s)
5_{ox}	(–0.91, –1.83)	1 982 (2 370)	526 (150, s)
		1 903 (2 060)	408 (540, s)
			258 (27 000, p)
			246 (24 000, v)
			228 (49 000, s)
5_{red}		1 963 (2 480)	440 (1 280, p)
		1 887 (2 100)	398 (1 090, v)
			324 (5 700, s)

[a] Potentials vs Fc/Fc^+ using 0.1 M $[n\text{-}Bu_4N]PF_6$. i and q denote irreversible and quasireversible, respectively. [b] p, v, and s denote peak, valley, and shoulder, respectively. [c] IR data obtained from a CH_2Cl_2 solution.

UV/Vis Absorption Spectroscopy. The oxidized states of free dppc and Re(dppc) carbonyl complexes all show tail absorption, to varying extents, into the visible region of the spectrum. Since the analogous Re(dppe) (dppe = 1,2-*bis*(diphenylphosphino)-

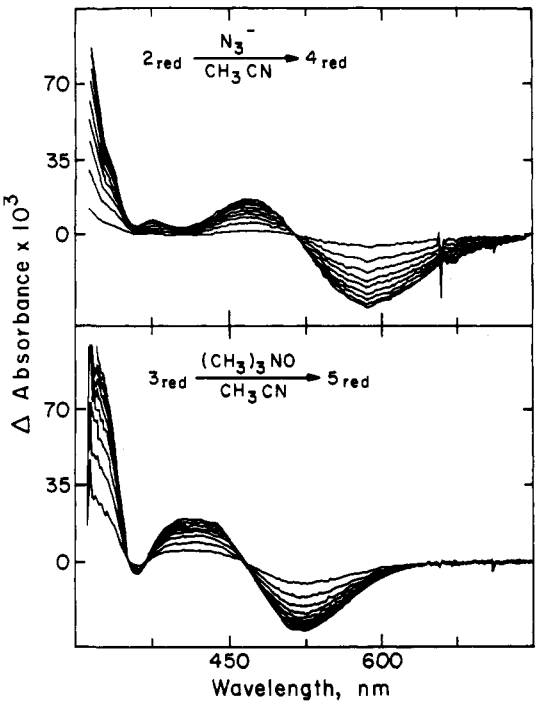

Figure 2. UV/visible spectral changes acquired using stopped flow techniques for the reaction of $\mathbf{2}_{red}$ (0.08 mM) with N_3^- (2 mM) to form $\mathbf{4}_{red}$ (top) and reaction of $\mathbf{3}_{red}$ (0.08 mM) with $(CH_3)_3NO$ (5 mM) to form $\mathbf{5}_{red}$ (bottom) in CH_3CN at 25.0 °C showing that, upon substitution of CO for less π-acidic ligands such as CH_3CN or NCO^-, the cobaltocene-based absorbance undergoes a hypsochromic shift. The presence of isosbestic points demonstrates absence of secondary reactions.

ethane) complexes are all white,[26] the visible absorption of the dppc complexes must be attributed to the colored cobaltocenium moiety. We find that the onset of visible absorption is ordered energetically according to the following: **2 > 3 > 4 > 5**. Our studies (*vide infra*) of reactivity toward nucleophiles (N_3^- or amine *N*-oxide) show that their electrophilicity shows the same order. Taking electrophilicity to reflect the extent to which the Re center is electron-poor, we suggest that the visible absorption of the oxidized complexes may have a component of Re(I) → Co(III) charge-transfer character. The first absorption of cobaltocenium which gives rise to its yellow color is a ligand field band and should not be affected significantly by variations in the ligands surrounding the Re center. Thus, while the lowest ligand field absorption of cobaltocenium is likely a component of the visible absorption of the oxidized complexes **2**, **3**, **4**, and **5**, the absorption also likely includes some Re(I) → Co(III) character.

For the reduced species **2**, **3**, **4**, and **5**, the absorptions dominating the visible region are lower in energy than for their oxidized analogues. This, too, follows the behavior of the absorption of cobaltocene vs cobaltocenium; the reduced species absorbs at longer wavelength. However, the nature of the Re fragment in the dppc complexes alters the position of the first absorption. We find that the first absorption energy is in the following order for the reduced complexes: **5 > 4 > 3 > 2**. Figure 2 shows UV/vis spectral changes upon reaction of $\mathbf{2}_{red}$ (60 μM in CH_3CN) with N_3^- and $\mathbf{3}_{red}$ (60 μM in CH_3CN) with $(CH_3)_3NO$. As the more π-acidic CO is substituted by more basic NCO^- or CH_3CN, the visible absorption band shifts to higher energy. From these observations it is reasonable to suggest that the visible absorption of the reduced Re(dppc) complexes possesses some Co(II) → Re(I) charge-transfer character, the excited state for which becomes higher in energy as the Re center is made more electron-rich.

Solution FTIR. FTIR spectra of the two states of charge of **2**, **3**, **4**, and **5** are shown in Figure 3 and tabulated in Table 2,

(26) Lorković, I. M.; Christ, C. S.; Wrighton, M. S. Unpublished results.

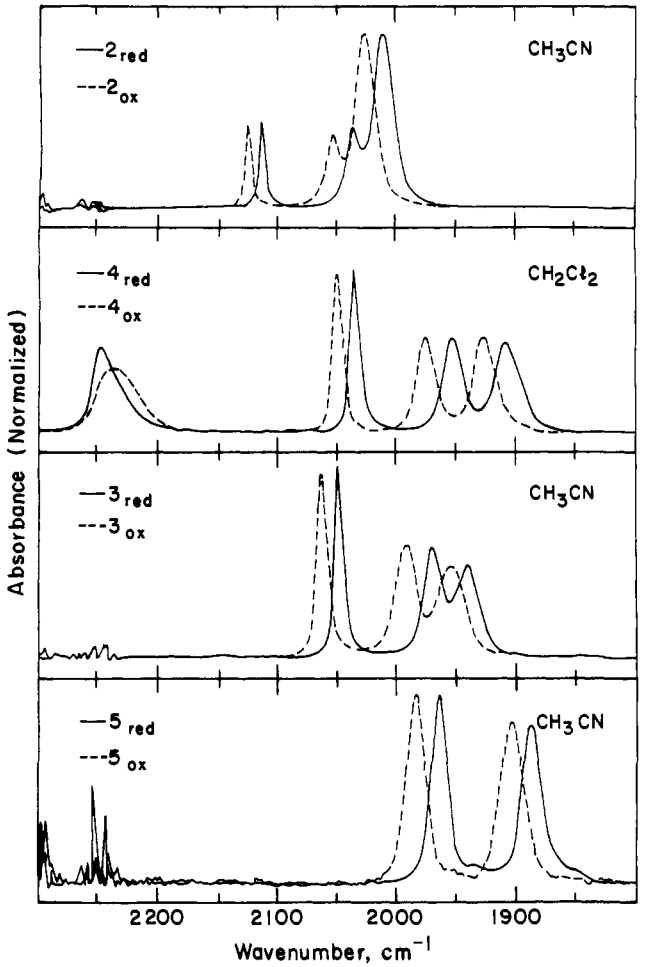

Figure 3. Solution IR spectra in the carbonyl region for **2**, **3**, **4**, and **5** showing that the spectra of the reduced forms of all species are identical to those of the oxidized forms except that all absorptions for the reduced species are ~15 cm^{-1} lower in energy.

and the data are characteristic of octahedral *cis*-tetracarbonyl (**2**), *fac*-tricarbonyl (**3** and **4**), and *cis*-dicarbonyl (**5**). Oxidizing the dppc ligand causes an increase in ν_{CO} of ~15 cm^{-1} with no change in the number or relative intensities of the absorptions. Thus, in solution, the steric properties of the two states of charge of **2** and **3** are, on average, effectively equivalent.

Kinetics. Part A: Reaction of 3 with Amine *N*-Oxides. Tertiary amine *N*-oxides have long been known as good oxygen atom transfer reagents, being more reactive than phosphine, arsine, or stibine oxides as a consequence of the absence of a low lying π-accepting empty d orbital on N, lending zwitterionic character to the N–O bond. Amine *N*-oxides are particularly reactive in the oxidation of transition metal bond CO to CO_2. More basic amine *N*-oxides are more reactive, and it is believed that nucleophilic attack of the oxide at the CO carbon is the rate limiting step.[12]

The kinetics results from studies of the reactions between **3** and amine *N*-oxides $(CH_3)_3NO$ (TMANO), *N*-methylmorpholine *N*-oxide (NMMNO), and *N*,*N*-dimethylaniline *N*-oxide (DMANO) in CH_3CN to form **5** are summarized in Table 3. The reactions were determined to be first order in **3** by virtue of the exponential absorbance rise and decay curves obtained under the pseudo-first-order conditions employed in this study. In addition, the pseudo-first-order rate constants observed for $\mathbf{3}_{ox}$ using [TMANO] = 0.504, 1.008, and 2.52 mM were 0.378, 0.771, and 2.00 s^{-1}, respectively, while those for $\mathbf{3}_{red}$ using [TMANO] = 13.9 and 21.8 mM were 0.059 and 0.083 s^{-1}, demonstrating that the reaction was also first order in TMANO. The reactions of $\mathbf{3}_{ox}$ with both NMMNO and DMANO were likewise found to

Table 3. Rate Constants and Activation Parameters for the Reaction between **3** and Amine *N*-Oxides[a] in CH_3CN (T = 25–39 °C)

	I, mM[b]	k_2 (25.0 °C), $M^{-1}\,s^{-1}$	k_{ox}/k_{red}	$\Delta H^{\ddagger}$ (σ), kcal/mol	$\Delta S^{\ddagger}$ (σ), eu
			TMANO		
3_{ox}	0.03	741	193	9.80 (47)	−12.7 (1.6)
3_{ox}	100[c]	621	156		
3_{red}	0.10	3.84		13.66 (44)	−10.1 (1.4)
3_{red}	100[c]	3.97			
			NMMNO		
3_{ox}	0.03	77.6	179	10.26 (49)	−15.5 (1.6)
3_{red}	0.10	0.433		13.34 (77)	−15.4 (2.5)
			DMANO		
3_{ox}	0.03	2 700	226	8.15 (47)	−15.5 (1.6)
3_{red}	0.10	11.9		9.31 (26)	−22.33 (86)

[a] TMANO, NMMNO, and DMANO are trimethylamine *N*-oxide, *N*-methylmorpholine *N*-oxide, and dimethylaniline *N*-oxide, respectively. [b] I is ionic strength. [c] [n-Bu_4N]PF_6 was used as the supporting electrolyte.

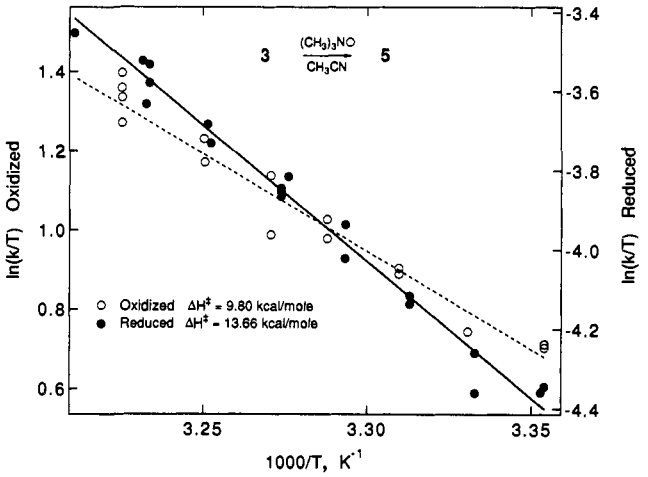

Figure 4. Eyring plot of the temperature-dependent rates of reaction between TMANO and 3_{ox} (open circles, left y-axis) and between TMANO and 3_{red} (filled circles, right y-axis) showing that reduction of the redox active ligand induces an increase in the activation enthalpy of nucleophilic attack at the carbonyl carbon atom of **3**.

Scheme 4. Reactivity Differences between 3_{ox} and 3_{red} with Amine-N-Oxides in CH_3CN at 25.0 °C

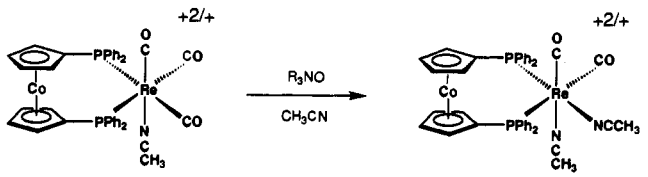

be first order in both *N*-oxides. The reduction of the dppc ligand causes approximately a 200-fold decrease in the rate constants for reactions between **3** and all three amine *N*-oxides (Table 3 and Scheme 4). Figure 4 shows the Eyring plots for the reactions between TMANO and both 3_{ox} and 3_{red}. The marked increase in the activation enthalpy (3.9 ± 0.9 kcal/mol) for the reaction upon reduction is evident. With NMMNO, for both states of charge of **3**, the reaction is 10 times slower and $\Delta S^{\ddagger}$ about 4 eu more negative than with TMANO, reflecting similar basicity for the two amine *N*-oxides and the bulkier nature of NMMNO. DMANO, despite its lower basicity, was the most reactive of the three amine *N*-oxides studied, as has previously been observed,[12b] reacting 4 times faster with **3** than TMANO. By imposing the condition that $\Delta S^{\ddagger}$ values for both states of charge be identical

Table 4. Rate Constants and Activation Parameters for the Reaction between **2** and N_3^- in CH_3CN (T = 25–39 °C)

	I, mM	k_2 (25.0 °C), $M^{-1}\,s^{-1}$	k_{ox}/k_{red}	$\Delta H^{\ddagger}$ (σ), kcal/mol	$\Delta S^{\ddagger}$ (σ), eu
2_{ox}	0.3	567 000	5 400	12.64 (23)	10.22 (75)
2_{red}	1.1	106		14.21 (47)	−1.6 (1.5)
2_{ox}	100[a]	72 000	2 200	13.31 (26)	7.86 (84)
2_{red}	100[a]	33		16.81 (47)	4.3 (1.6)

[a] [n-Bu_4N]PF_6 was used as the supporting electrolyte.

Scheme 5. Reactivity Differences between 2_{ox} and 2_{red} with N_3^- in CH_3CN at 25.0 °C

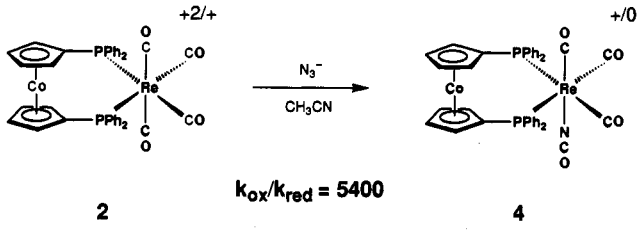

in the reactions of **3** with the amine *N*-oxides studied, the reactivity differences observed correspond to a $\Delta\Delta H^{\ddagger}$ of 3.1–3.2 kcal/mol.

The reaction between 3_{ox} and TMANO proceeded at a 14 ± 5% slower rate in CH_3CN containing 0.1 M [n-Bu_4N]PF_6 at 25 °C, while the same reaction with 3_{red} was unaffected by the presence of electrolyte. These results, compared to the strong ionic strength dependence of the reactions between **2** and N_3^- (*vide infra*), are consistent with the activated complex bearing the same overall charge as the dicationic reactant.

An interesting property of the reaction of 3_{ox} with TMANO is that at $T < 20$ °C or higher concentrations of TMANO, with no change in the yield of 5_{ox}, the absorbance change with time exhibits biexponential behavior. Accumulation of a significant concentration of the putative intermediate rhenium (*O*-trimethylamino) carboxylate (eq 2), which to our knowledge has never been directly observed, is consistent with these observations. Another possibility is that the intermediate is the $N(CH_3)_3$ complex. A low-temperature spectral study of this reaction would be instructive in this regard.

Part B: Reaction of 2 with the Anionic Nucleophile N_3^-. Azide anion reacts with metal carbonyls in a fashion similar to amine *N*-oxides in that the rate limiting step is thought to be nucleophilic attack at the CO carbon.[9] A rapid Curtius type rearrangement is postulated to follow, giving the metal isocyanate and free N_2. At 25 °C in CH_3CN the reaction between **2** and N_3^- to form **4** was found to be first order in **2** by virtue of the exponential absorbance rise and decay curves observed under pseudo-first-order conditions. In addition, the pseudo-first-order rate constants, corrected for ionic strength differences (*vide infra*), observed for 2_{ox} using $[N_3^-]$ = 0.21, 0.42, and 0.82 mM were 150, 270, and 560 s^{-1}, respectively, while those for 2_{red} using $[N_3^-]$ = 1.00 and 3.27 mM were 0.106 and 0.324 s^{-1}, respectively, demonstrating that the reaction was also first order in N_3^-. 2_{ox} reacts with N_3^- 5400 times faster than 2_{red} (Table 4 and Scheme 5). In a 0.1 M [n-Bu_4N]PF_6/CH_3CN solution, however, 2_{ox} and 2_{red} react 8 and 3 times slower, respectively, with N_3^- than with no supporting electrolyte, and the redox-induced rate constant change is only a factor of 2200. The Eyring plots for the reactions between both states of charge of **2** and N_3^- in CH_3CN/0.1 M [n-Bu_4N]PF_6 are shown in Figure 5, and the activation parameters for both media are summarized in Table 4. Similar to what was observed for the reaction between **3** and TMANO, $\Delta H^{\ddagger}$ is 3.5 ± 0.7 kcal/mol higher for the reaction of the reduced form of the species. Considering the relative rates of reaction of the oxidized and reduced Re species with the neutral amine *N*-oxides (*vide supra*) the enhancement in the reaction rate of 2_{ox} with N_3^- over that of 2_{red} is greater than one might expect solely on the basis

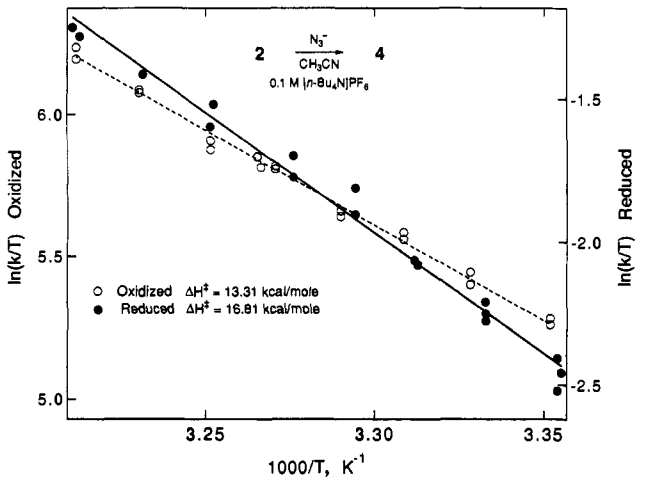

Figure 5. Eyring plot of the temperature-dependent rates of reaction between N_3^- and $\mathbf{2}_{ox}$ (open circles, left y-axis) and between N_3^- and $\mathbf{2}_{red}$ (filled circles, right y-axis) showing that reduction of the redox active ligand induces an increase in the activation enthalpy of nucleophilic attack at the carbonyl carbon atom of **2**.

of $\Delta\nu_{CO} = 15\ cm^{-1}$. We attribute the additional enhancement to the fact that N_3^- is negatively charged. It is important to realize that the electrostatic effect is at least partly derived from changes in positive charge localized in the dppc ligand, the center (Co atom) of which is 4.4 Å from the Re atom. In order to better understand the enhanced reactivity due to the electrostatic attraction between $dppc^+$ in $\mathbf{2}_{ox}$ and N_3^-, the ionic strength (I) and dielectric strength (ϵ) dependencies of the rate of reaction between **2** and N_3^- were investigated.

The Brønsted primary salt effect,[27,28] described by eq 3 for a solution in which all ions are dissociated, dictates that, as I (de-

$$\ln k = \ln k_{I=0} - 2Az_az_bI^{1/2} \qquad (3)$$

$$A = (0.056\ 28)F^3N_A^{-1}(\epsilon\epsilon_0RT)^{-3/2}$$

fined here as having units of mol/dm³) approaches 0, ln k should change linearly with $I^{1/2}$, where F is 96 485 C mol^{-1}, N_A is 6.022 × 10^{23} mole^{-1}, and ϵ_0 is 8.854 × 10^{-12} C^2 J^{-1} m^{-1}. For CH_3CN at 25.0 °C (ϵ = 36.7),[30] A is 3.67. Figure 6 shows theoretical and experimental plots for the reactions between N_3^- and both states of charge of **2** as a function of the concentration of [n-Bu_4N]-PF_6 supporting electrolyte. The observed $I^{1/2}$ dependence of ln k, at I < 20 mM, agrees well with the predicted slopes of −7.34 for $\mathbf{2}_{red}$ and −14.68 for $\mathbf{2}_{ox}$. These results are consistent with all ions in solution being dissociated and the activity of $\mathbf{2}_{ox}$ being of a dication. The ionic strength dependence of the reactivity of $\mathbf{2}_{ox}$ is expected to be typical of a dication because the Debye length is at least 10 Å for the conditions used in this study,[28] significantly longer than the Co to CO carbon distance (4.8 Å). The Debye length characterizes distances over which the ionic atmosphere stabilizes the charged reactant and activated complexes.

The dielectric strength dependence of the reactivity between ions has been approximated by the "double sphere" [27] model (eq 4), which predicts a linear relationship between ln k and ϵ^{-1},

$$\ln k = \ln k_\infty - 1/\epsilon(z_az_be^2/4\pi\epsilon_0d_{ab}kT) \qquad (4)$$

where k_∞ is the rate constant in a medium of infinite dielectric strength. The apparent center-to-center distance between the ions in the activated complex, d_{ab}, can be calculated from the

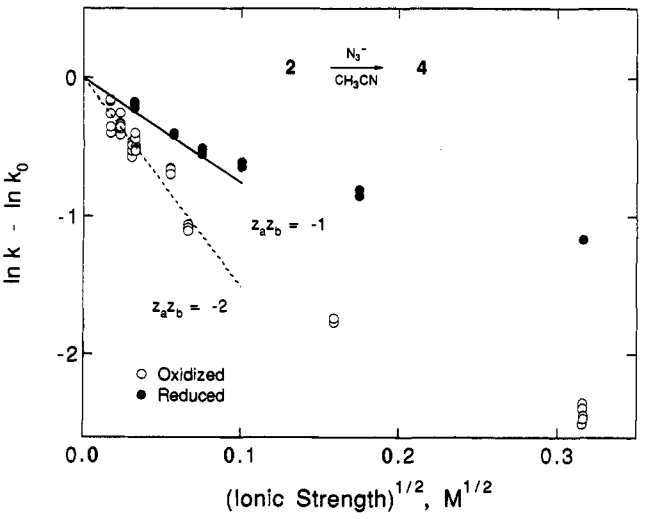

Figure 6. Ionic strength dependence of the reaction between N_3^- and $\mathbf{2}_{ox}$ (open circles) and N_3^- and $\mathbf{2}_{red}$ (filled circles). Shown are ionic strength dependencies for a biomolecular reaction between a cation and an anion (solid line) and between a dication and an anion (dashed line) predicted by the Debye–Hückel limiting law in a medium having ϵ of 36.7 at 25.0 °C.

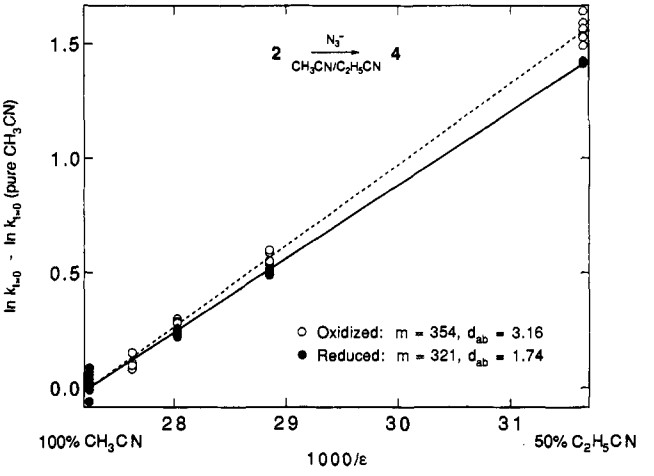

Figure 7. Dielectric strength dependence of the reactions between N_3^- and $\mathbf{2}_{ox}$ (open circles) and N_3^- and $\mathbf{2}_{red}$ (filled circles) at 25.0 °C. For this figure the dielectric strength is decreased by addition of C_2H_5CN, and it is assumed that the dielectric strength of the mixture is linearly dependent on the volume percent of C_2H_5CN. The best fit slopes for $\mathbf{2}_{ox}$ and $\mathbf{2}_{red}$ are 354 and 321, corresponding to d_{ab} = 3.16 and 1.74 Å, respectively.

slope of the line obtained by plotting ln $k_{I=0}$ (obtained by extrapolating the observed rate constants at non-zero ionic strength to I = 0 using eq 3) vs ϵ^{-1}. Figure 7 shows a plot of ln $k_{I=0}$ vs ϵ^{-1} for the reaction between **2** and N_3^-. In this experiment, ϵ was varied by preparation of CH_3CN solutions containing different volume percentages of C_2H_5CN (ϵ = 26.5 at 25.0 °C) and assuming that ϵ is a linear function of the volume (or mass, since $\rho(CH_3CN) = 0.786$ g/mL ≈ $\rho(C_2H_5CN) = 0.782$ g/mL) percent composition of the binary mixture. In this case, oxidizing dppc increases the slope by only 10 ± 2% (from 321 to 354), giving apparent d_{ab} values of 1.74 and 3.16 Å for $\mathbf{2}_{red}$ and $\mathbf{2}_{ox}$, respectively. A possible explanation for the fact that the ϵ dependence of the reaction of **2** with N_3^- is relatively insensitive to the state of charge of the dppc ligand is that the distances characterizing the relative dielectric stabilization of the electrostatic potential energies of the reactants and activated complex are on the order of d_{ab} (~2 Å), which is considerably shorter than the Co to CO carbon distance (~4.8 Å). Thus, $\mathbf{2}_{ox}$ behaves as a molecule containing two separate monocationic centers in the ϵ dependence

(27) Laidler, K. J. *Chemical Kinetics*; McGraw Hill: New York, 1965; Chapter 5.
(28) Atkins, P. W. *Physical Chemistry*; W. H. Freeman: New York, 1986; Chapter 11.
(29) Amis, E. S.; La Mer, V. K. *J. Am. Chem. Soc.* **1939**, *61*, 905.

of its reactivity with N_3^-, in contrast to the behavior upon variation in ionic strength, where $\mathbf{2}_{ox}$ behaves as a simple dication.

The activation parameters measured at low ionic strength ($\Delta H^{\ddagger}_{obs}$ and $\Delta S^{\ddagger}_{obs}$) for the reaction between **2** and N_3^- shown in Table 4 may be separated into electrostatic (es) and nonelectrostatic (nes) contributions (eqs 5 and 6). Since the reaction of

$$\Delta H^{\ddagger}_{obs} = \Delta H^{\ddagger}_{es} + \Delta H^{\ddagger}_{nes} \quad (5)$$

$$\Delta S^{\ddagger}_{obs} = \Delta S^{\ddagger}_{es} + \Delta S^{\ddagger}_{nes} \quad (6)$$

$\mathbf{2}_{ox}$ and $\mathbf{2}_{red}$ with N_3^- is between ions, both reactions have significant $\Delta H^{\ddagger}_{es}$ and $\Delta S^{\ddagger}_{es}$. We take the difference in these parameters between the states of charge of **2** ($\Delta\Delta H^{\ddagger}_{es}$ and $\Delta\Delta S^{\ddagger}_{es}$) eqs 7 and 8) to be the additional electrostatic contribution caused by changing the charge on the dppc ligand.

$$\Delta\Delta H^{\ddagger}_{es} = \Delta H^{\ddagger}_{es}(\mathbf{2}_{ox}) - \Delta H^{\ddagger}_{es}(\mathbf{2}_{red}) \quad (7)$$

$$\Delta\Delta S^{\ddagger}_{es} = \Delta S^{\ddagger}_{es}(\mathbf{2}_{ox}) - \Delta S^{\ddagger}_{es}(\mathbf{2}_{red}) \quad (8)$$

The rate constant for reaction between ions as a function of temperature, but at constant ϵ (by using different solvent mixtures), gives the nonelectrostatic activation parameters.[29] Unfortunately, data are not available regarding the temperature dependence of ϵ for the binary mixtures of CH_3CN and C_2H_5CN we have used. However, the essential information can be obtained from our data, because the temperature dependence of ϵ for CH_3CN is known[30] and we have measured the ϵ dependence of the rate of reaction between **2** and N_3^- at a fixed temperature (Figure 7). Thus, according to the literature,[29] we find $\Delta H^{\ddagger}_{nes}$ = 10.22 ± 0.23 and 12.02 ± 0.47 kcal/mol and $\Delta S^{\ddagger}_{nes}$ = −15.83 ± 0.75 and −25.2 ± 1.5 eu for $\mathbf{2}_{ox}$ and $\mathbf{2}_{red}$, respectively. Furthermore, using eqs 5–8, $\Delta\Delta H^{\ddagger}_{es}$ = 0.23 kcal/mol and $\Delta\Delta S^{\ddagger}_{es}$ = 2.45 e.u., leading to the conclusion that there is a 5-fold overall electrostatic rate enhancement in the relative reactivity of $\mathbf{2}_{ox}$ to $\mathbf{2}_{red}$ with N_3^-. Hence, the nonelectrostatic rate constant ratio between $\mathbf{2}_{ox}$ and $\mathbf{2}_{red}$ in the reaction with N_3^- is approximately 1100 ($\Delta\Delta H^{\ddagger}_{nes}$ = 4.1 kcal/mol, assuming $\Delta\Delta S^{\ddagger}$ = 0) at 25 °C.

(30) Maryott, A. A.; Smith, E. R. *Table of Dielectric Constants of Pure Liquids*; NBS Circular #514; U.S. Government Printing Office: Washington, DC, 1951.

Conclusions

Using the reversibly redox-active chelating cobaltocene ligand dppc, we have demonstrated electrochemical control of the reactivity of a Re carbonyl moiety toward nucleophilic attack at a carbonyl carbon atom. Ligand (dppc) oxidation by one electron results in a $\Delta\nu_{CO}$ of ~15 cm^{-1}, a ~200-fold increase in reactivity of **3** with tertiary amine *N*-oxides, a 5400-fold increase in reactivity of **2** with N_3^-, and, for both reactions, a 3–4 kcal/mol decrease in $\Delta H^{\ddagger}$. The reactivity of **2** with N_3^- displays a classic Brønsted primary salt effect, with $\mathbf{2}_{ox}$ subject to twice the ionic strength dependence of $\mathbf{2}_{red}$, but minimal change in dielectric strength dependence upon ligand oxidation.

Acknowledgment. We thank the National Science Foundation for support of this research. I.M.L. thanks the National Science Foundation for a Predoctoral Fellowship. We also thank Dr. Joseph M. Bollinger, Jr., Mr. Wei Wu, and Professor JoAnne Stubbe for the loan of, and assistance in using, the stopped flow instruments, and we thank Dr. Daniel Giaquinta for assistance with the crystallography.

Supplementary Material Available: Tables listing experimental details of the crystal structures of $\mathbf{2}_{ox}$ and $\mathbf{2}_{red}$, including atom positional parameters, B(eq) values, bond lengths, bond angles, and least-squares plane information (11 pages). This material is contained in many libraries on microfiche, immediately follows this article in the microfilm version of the journal, and can be ordered from the ACS; see any current masthead page for ordering information.